Targeting of the Cholecystokinin-2 Receptor with the Minigastrin Analog ^{177}Lu-DOTA-PP-F11N: Does the Use of Protease Inhibitors Further Improve In Vivo Distribution?

Alexander W. Sauter*[1,2], Rosalba Mansi*[3], Ulrich Hassiepen[4], Lionel Muller[4], Tania Panigada[4], Stefan Wiehr[2], Anna-Maria Wild[2], Susanne Geistlich[5], Martin Béhé[5], Christof Rottenburger[1], Damian Wild[1], and Melpomeni Fani[3]

[1]Division of Nuclear Medicine, University Hospital Basel, Basel, Switzerland; [2]Werner Siemens Imaging Center, Department of Preclinical Imaging and Radiopharmacy, Eberhard Karls University, Tuebingen, Germany; [3]Division of Radiopharmaceutical Chemistry, University Hospital Basel, Basel, Switzerland; [4]Novartis Pharma AG, Institutes for Biomedical Research, Novartis Campus, Basel, Switzerland; and [5]Center for Radiopharmaceutical Sciences, Paul Scherrer Institute, Villigen, Switzerland

Patients with metastatic medullary thyroid cancer (MTC) have limited systemic treatment options. The use of radiolabeled gastrin analogs targeting the cholecystokinin-2 receptor (CCK2R) is an attractive approach. However, their therapeutic efficacy is presumably decreased by their enzymatic degradation in vivo. We aimed to investigate whether the chemically stabilized analog ^{177}Lu-DOTA-PP-F11N (^{177}Lu-DOTA-(DGlu)$_6$-Ala-Tyr-Gly-Trp-Nle-Asp-Phe-NH$_2$) performs better than reference analogs with varying in vivo stability, namely ^{177}Lu-DOTA-MG11 (^{177}Lu-DOTA-DGlu-Ala-Tyr-Gly-Trp-Met-Asp-Phe-NH$_2$) and ^{177}Lu-DOTA-PP-F11 (^{177}Lu-DOTA-(DGlu)$_6$-Ala-Tyr-Gly-Trp-Met-Asp-Phe-NH$_2$), and whether the use of protease inhibitors further improves CCKR2 targeting. First human data on ^{177}Lu-DOTA-PP-F11N are also reported. **Methods:** In vitro stability of all analogs was assessed against a panel of extra- and intracellular endoproteases, whereas their in vitro evaluation was performed using the human MTC MZ-CRC-1 and the transfected A431-CCK2R(+) cell lines. Biodistribution without and with the protease inhibitors phosphoramidon and thiorphan was assessed 4 h after injection in MZ-CRC-1 and A431-CCK2R(+) dual xenografts. Autoradiography of ^{177}Lu-DOTA-PP-F11N (without and with phosphoramidon) and NanoSPECT/CT were performed. SPECT/CT images of ^{177}Lu-DOTA-PP-F11N in a metastatic MTC patient were also acquired. **Results:** ^{nat}Lu-DOTA-PP-F11N is less of a substrate for neprilysins than the other analogs, whereas intracellular cysteine proteases, such as cathepsin-L, might be involved in the degradation of gastrin analogs. The uptake of all radiotracers was higher in MZ-CRC-1 tumors than in A431-CCK2R(+), apparently because of the higher number of binding sites on MZ-CRC-1 cells. ^{177}Lu-DOTA-PP-F11N had the same biodistribution as ^{177}Lu-DOTA-PP-F11; however, uptake in the MZ-CRC-1 tumors was almost double (20.7 ± 1.71 vs. 11.2 ± 2.94 %IA [percentage injected activity]/g, $P = 0.0002$). Coadministration of phosphoramidon or thiorphan increases ^{177}Lu-DOTA-MG11 uptake significantly in the CCK2R(+) tumors and stomach. Less profound was the effect on ^{177}Lu-DOTA-PP-F11, whereas no influence or even reduction was observed for ^{177}Lu-DOTA-PP-F11N (20.7 ± 1.71 vs. 15.6 ± 3.80 [with phosphoramidon] %IA/g, $P < 0.05$ in MZ-CRC-1 tumors). The first clinical data show high ^{177}Lu-DOTA-PP-F11N accumulation in tumors, stomach, kidneys, and colon. **Conclusion:** The performance of ^{177}Lu-DOTA-PP-F11N without protease inhibitors is as good as the performance of ^{177}Lu-DOTA-MG11 in the presence of inhibitors. The human application of single compounds without unessential additives is preferable. Preliminary clinical data spotlight the stomach as a potential dose-limiting organ besides the kidneys.

Key Words: medullary thyroid cancer; cholecystokinin-2 receptor; gastrin; peptide receptor radionuclide therapy; ^{177}Lu-DOTA-PP-F11N

J Nucl Med 2019; 60:393–399
DOI: 10.2967/jnumed.118.207845

Medullary thyroid cancer (MTC) is a neuroendocrine neoplasm that is initially treated with complete thyroidectomy and at least central neck dissection (*1*). However, patients with residual or recurrent disease are difficult to treat (*2,3*), and distant metastases are the main cause of death. Systemic chemotherapy has shown limited efficacy for the treatment of advanced and metastatic disease (*4*). Targeted therapies, such as vandetanib and cabozantinib, show a broad spectrum of side effects, often leading to discontinuation or dose reduction (*2*), whereas no improvement in overall survival has been shown until now (*3*).

Almost all MTC cells (92%) express the cholecystokinin-2 receptor (CCK2R) with high density (*5*). Peptide receptor radionuclide therapy with radiolabeled analogs of the endogenous ligand gastrin does specifically target the CCK2R and is therefore an attractive treatment option for MTC. The 2 main drawbacks of radiolabeled gastrin analogs are high retention in the kidneys and low in vivo stability (*6,7*). Both limitations have been addressed by different groups applying alternative chemical modifications (*8*). Supported by the European Cooperation in Science and Technology action BM0607, a large library of improved gastrin analogs has been compared (*9–11*). Among them, the analog PP-F11 ((DGlu)$_6$-Ala-Tyr-Gly-Trp-Met-Asp-Phe-NH$_2$), resulted in favorable pharmacokinetics, relatively low kidney uptake, and improved metabolic stability. ^{111}In-DOTA-PP-F11 was selected for evaluation in MTC patients within the framework of a multinational European cooperation project (TRANSCAN call within ERANET, project GRAN-T-MTC). Replacement of methionine in PP-F11 by the nonoxidizing amino acid residue norleucine, a known strategy to circumvent undesired methionine oxidation side-reactions, results in the stabilized derivative PP-F11N ((DGlu)$_6$-Ala-Tyr-Gly-Trp-Nle-Asp-Phe-NH$_2$).

Received Jan. 4, 2018; revision accepted Jun. 29, 2018.
For correspondence or reprints contact: Melpomeni Fani, Division of Radiopharmaceutical Chemistry, University Hospital Basel, University of Basel, Petersgraben 4, 4031 Basel, Switzerland.
E-mail: melpomeni.fani@usb.ch
*Contributed equally to this work.
Published online Jul. 12, 2018.

In addition to chemical modifications, Nock et al. proposed a pharmacologic approach for improving in vivo stability (*12*). They demonstrated in an animal model that coinjection of phosphoramidon, an inhibitor of the neprilysin (NEP), with the unstable minigastrin analog ^{111}In-DOTA-MG11 (^{111}In-DOTA-DGlu-Ala-Tyr-Gly-Trp-Met-Asp-Phe-NH_2) leads to profound in vivo stabilization and subsequently to a significant increase in tumor uptake. In addition, NEP inhibition using thiorphan and its prodrug racecadotril significantly enhances the tumor-to-kidney ratios (*13*). The in vivo inhibition of degrading enzymes appears to be promising, especially when further chemical modifications cannot be conducted without abolishing biologic activity or preferred pharmacokinetic properties.

We are interested in applying peptide receptor radionuclide therapy in MTC patients. We aimed to investigate whether the peptide stabilization approach or in situ stabilization by the use of protease inhibitors or the combination of both can optimize CCK2R targeting in vivo. We selected the chemically stabilized ^{177}Lu-DOTA-PP-F11N (^{177}Lu-DOTA-(DGlu)$_6$-Ala-Tyr-Gly-Trp-Nle-Asp-Phe-NH_2) as a therapeutic agent and compared it with 2 gastrin analogs with varying stability in vivo, namely ^{177}Lu-DOTA-MG11 and ^{177}Lu-DOTA-PP-F11 (^{177}Lu-DOTA-(DGlu)$_6$-Ala-Tyr-Gly-Trp-Met-Asp-Phe-NH_2). In vitro stability, tissue biodistribution, and tumor uptake were investigated without and with the use of the 2 protease inhibitors phosphoramidon and thiorphan. In vivo comparison was performed in 2 xenografted models using the transfected epidermoid carcinoma cell line A431, expressing the human CCK2R [A431-CCK2R(+)] and the MZ-CRC-1 derived from human MTC, naturally expressing the CCK2R. Finally, we report herein the first human data of ^{177}Lu-DOTA-PP-F11N in an MTC patient as part of an ongoing clinical phase 0 study (LUMED trial, NCT02088645).

MATERIALS AND METHODS

Reagents and Cell Lines

DOTA-MG11, DOTA-PP-F11, and DOTA-PP-F11N were custom-made by Biosyntan GmbH. All reagents were obtained from commercial suppliers.

The A431-CCKR(−) and A431-CCK2R(+) cell lines were kindly provided by Dr. Luigi Aloj and cultured as previously reported (*14*). The MZ-CRC-1 cell line was provided by Prof. Alexander Knuth and maintained in DMEM high-glucose, 4.5 g/L, supplemented with 20 mM L-glutamine and 10% fetal bovine serum.

Preparation of $^{nat/177}$Lu Conjugates

^{177}Lu labeling was performed by dissolving 5 μg of the DOTA conjugates in 250 μL of sodium acetate buffer (0.4 M, pH 5.0), followed by incubation with $^{177}LuCl_3$ (40–150 MBq) for 30 min at 95°C. Methionine (50 μL, 0.1 M) was added to DOTA-MG11 and DOTA-PP-F11 to eliminate oxidation. The radiotracer solutions were used without further purification and were diluted with 0.9% NaCl containing 0.05% human serum albumin for in vivo use. ^{nat}Lu complexes were prepared under the same conditions, using a 2.5-fold excess of $^{nat}LuCl_3 \times 5H_2O$, and were purified by SepPak (Waters).

In Vitro Stability Assessment

The stability of ^{nat}Lu-loaded peptides was tested against the active forms of selected human aspartic, cysteine, and metalloproteases in vitro. Each analog (20 μM) was incubated with the listed proteases. The enzyme concentrations and buffers were as follows: for angiotensin-converting enzyme 1, 25 nM neprilysin-1 and neprilysin-2, pH 7.4 phosphate-buffered saline, and 0.05% 3-[(3-cholamidopropyl)dimethylammonio]-1-propanesulfonate (CHAPS); for endothelin-converting enzyme 1, 25 nM and 50 mM pH 7.4 tris(hydroxymethyl)aminomethane (Tris)/HCl, 150 mM NaCl, and 0.05% CHAPS; for aminopeptidase-N and aminopeptidase-P2, 25 nM and 50 mM pH 7.4 Tris/HCl and 0.05% CHAPS; and for cathepsin-B, -C, -K, -L, and -S, 50 nM and 100 mM pH 5.5 sodium acetate, 100 mM NaCl, 1 mM ethylenediaminetetraacetic acid, 2 mM (tris(2-carboxyethyl)phosphine), and 0.05% CHAPS.

After 2.5 h of incubation in polypropylene tubes at room temperature, the samples were analyzed for peptide cleavage by liquid chromatography/mass spectrometry. Intact peptides and the cleavage products were detected by the ultraviolet absorption (214 nm), and their mass was determined by electrospray ionization quadrupole time-of-flight mass spectrometry. Their amino acid sequences were determined using Protein Analysis Work Sheet software (Proteometrics Inc.).

Analytic Methods and Instrumentation

Liquid chromatography/mass spectrometry was performed on an Acquity ultraperformance liquid chromatography system (Waters Corp.) equipped with an Acquity ultraperformance liquid chromatography Cortecs C18 (2.1 × 100 mm; 1.6 μm) column. Eluent A was water with 0.05% (v/v) trifluoroacetic acid, and eluent B was acetonitrile with 0.04% (v/v) trifluoroacetic acid. The samples were run with a 5%–98% eluent B gradient in 4.4 min and a flow rate of 0.8 mL/min.

Mass spectrometry analysis was performed with the following conditions. The electrospray ionization quadrupole time-of-flight source temperature was set at 130°C, the desolvation temperature was set at 500°C, the capillary voltage was set at 3.00 kV, and the cone voltage was set at 30 V. The scan time was set at 0.1 s. The cone gas flow was set at 50 L/h and the desolvation gas flow at 800 L/h. The mass chromatograms were recorded in total ion current within 120 m/z and 3,000 m/z.

Analytical reverse-phase high-performance liquid chromatography was performed on a Bischoff LC-CaDi 22-14 interface with an ultraviolet–visible Lambda 1010 detector and a flow-through Berthold LB509 γ-detector using a Phenomenex Jupiter Proteo 90 Å C12 (250 × 4.6 mm) column. The following elution system was used: eluent A was water with 0.1% trifluoroacetic acid, eluent B was acetonitrile with 0.1% trifluoroacetic acid, gradient 1 was 70%–55% solvent A in 10 min, and the flow rate was 1.5 mL/min.

Quantitative γ-counting was performed on a Cobra 5003 γ-system well counter from Packard Instruments.

Binding and Internalization Studies

Saturation binding studies of $^{177/nat}$Lu-DOTA-MG11, $^{177/nat}$Lu-DOTA-PP-F11, and $^{177/nat}$Lu-DOTA-PP-F11N (concentration range, 0.1–100 nM) were performed on MZ-CRC-1 and A431-CCK2R(+) cells (1×10^6 cells per well) in 6-well plates, as previously described (*14*).

The internalization rate of ^{177}Lu-DOTA-PP-F11N, compared with ^{177}Lu-DOTA-MG11, was determined in MZ-CRC-1 cells, as previously described (*7*).

Biodistribution Studies

Animals were housed and cared according to Swiss regulations on animal experimentation (approval 2756). Female athymic nude-*Foxn1*^{nu} mice, 4–6 wk old, were inoculated subcutaneously in the right shoulder with 5×10^6 MZ-CRC-1 cells and 2 d later in the left shoulder with 5×10^6 A431-CCK2R(+) cells, both freshly suspended in sterile phosphate-buffered saline. The tumors were allowed to grow for 9 and 7 d, respectively, reaching a weight of 107 ± 57 mg (MZ-CRC-1) and 129 ± 36 mg (A431-CCK2R(+)).

The biodistribution of ^{177}Lu-DOTA-MG11, ^{177}Lu-DOTA-PP-F11, and ^{177}Lu-DOTA-PP-F11N was evaluated 4 h after injection of 100 μL/10 pmol/0.2–0.3 MBq of each radiotracer via the tail vein. The influence of phosphoramidon (phosphoramidon disodium dehydrate; PeptaNova) and thiorphan (DL-thiorphan; Bachem) was evaluated at 4 h by coinjection of either 300 μg of phosphoramidon in

phosphate-buffered saline or thiorphan in phosphate-buffered saline/5%–7% ethanol. The nonspecific uptake of ^{177}Lu-DOTA-PP-F11N was determined in A431-CCK2R(−) xenografts (Supplemental Table 1; supplemental materials are available at http://jnm.snmjournals.org). Blood samples and organs of interest were collected, blotted dry, weighed, and counted in a γ-counter. The results were expressed as mean ± SD and represent the percentage injected activity per gram of tissue (%IA/g).

NanoSPECT/CT Imaging and Autoradiography

Mice were imaged using a NanoSPECT/CT system (Bioscan) 4 h after injection of 100 μL/100 pmol/6 MBq of ^{177}Lu-DOTA-PP-F11N without or with 300 μg of phosphoramidon. Topography and helical CT were first performed. A helical SPECT scan was then acquired using multipurpose pinhole collimators (aperture 1) with a 1.4-mm pinhole diameter. The energy window width was 10% centered symmetrically over the 208- and 113-keV γ-peaks of ^{177}Lu. Forty projections, 500 s each, were used. SPECT images were reconstructed iteratively and filtered using the manufacturer's algorithm, resulting in a pixel size of 0.2 × 0.2 mm.

Tumors were dissected and embedded in optimal-cutting-temperature compound (Tissue-Tek; Sakura) and snap-frozen. Cryosections of 20-μm thickness were exposed for 24 h to phosphor screens, and autoradiograms were acquired with a storage phosphor imager (445SI; Molecular Dynamics) with spatial resolution of 50 μm. The data were analyzed using ImageJ software (National Institutes of Health). The same tissue slices were stained with hematoxylin and eosin following standard procedures. The slides were scanned using the digital slide scanner NanoZoomer 2.0-HT (Hamamatsu Photonics K.K.).

First-in-Human Application of ^{177}Lu-DOTA-PP-F11N

As part of the LUMED trial, the scan results of a 40-y-old man with progressive, metastatic MTC are presented in a comparison of ^{177}Lu-DOTA-PP-F11N SPECT and SPECT/CT with ^{18}F-DOPA PET and PET/CT. ^{177}Lu-DOTA-PP-F11N (20 mL, 95 μg, 1,071 MBq) was injected intravenously. SPECT/CT of the neck, thorax, and abdomen was performed 24 h after injection using a Symbia Intevo SPECT/CT system (Siemens Healthineers). SPECT was performed in a 128 × 128 matrix, with 64 views of 20 s each. SPECT images were reconstructed with iterative ordered-subset expectation maximum using a Flash 3D algorithm (8 iterations, 4 subsets, and 8-mm gaussian filtering). ^{18}F-DOPA PET with contrast medium–enhanced CT was done according to the European Association of Nuclear Medicine guidelines without carbidopa (*15*). Thirty minutes after injection of 228 MBq of ^{18}F-DOPA, 3-dimensional whole-body (head to subinguinal region) PET/CT was performed (Biograph mCT X128; Siemens Healthineers). The institutional review board approved this study, and the patient gave written informed consent in accordance with the Declaration of Helsinki.

Statistical Analysis

Comparisons were performed using the unpaired Student *t* test for normally distributed data, as previously tested with a Shapiro–Wilk normality test. The Mann–Whitney *U* test was applied for nonnormally distributed data. Statistical significance was defined at a *P* level of 0.05 or less.

RESULTS

Radiotracers

All radiotracers were produced with a radiolabeling yield of more than 95%. Radiochemical purity was at least 95% for ^{177}Lu-DOTA-PP-F11N but slightly lower (≥92%) for ^{177}Lu-DOTA-MG11 and ^{177}Lu-DOTA-PP-F11, due to the methionine oxidized product, which in all cases was kept to less than 5%.

In Vitro Stability Assessment

Table 1 shows the identified fragments of the ^{nat}Lu conjugates after incubation with human proteases in vitro. All were found to be stable in the presence of angiotensin-converting enzyme 1, endothelin-converting enzyme 1, aminopeptidase-N, and aminopeptidase-P2. ^{nat}Lu-DOTA-MG11 was found to be cleaved by neprilysin-1 and neprilysin-2 and the cathepsins -B, -C, -L and -S, ^{nat}Lu-DOTA-PP-F11 by neprilysin-1 and cathepsin-L, whereas ^{nat}Lu-DOTA-PP-F11N was degraded by the cysteine protease cathepsin-L only.

TABLE 1
Cleavage Sites in ^{nat}Lu-DOTA-MG11, ^{nat}Lu-DOTA-PP-F11, and ^{nat}Lu-DOTA-PP-F11N After Incubation with Selected Proteases

Gastrin analog	Protease	Detected peptide sequences
^{nat}Lu-DOTA-MG11	None	^{nat}Lu-DOTA-DGlu-Ala-Tyr-Gly-Trp-Met-Asp-Phe-NH_2
	Neprilysin-1	^{nat}Lu-DOTA-DGlu-Ala-Tyr-Gly ↓ Trp-Met-Asp ↓ Phe-NH_2
	Neprilysin-2	^{nat}Lu-DOTA-DGlu-Ala-Tyr-Gly ↓ Trp-Met-Asp-Phe-NH_2
	Cathepsin-B	^{nat}Lu-DOTA-DGlu-Ala-Tyr-Gly-Trp-Met-Asp ↓ Phe-NH_2
	Cathepsin-C	^{nat}Lu-DOTA-DGlu-Ala-Tyr-Gly-Trp-Met ↓ Asp-Phe-NH_2
	Cathepsin-L	^{nat}Lu-DOTA-DGlu-Ala-Tyr-Gly-Trp-Met ↓ Asp-Phe-NH_2
	Cathepsin-S	^{nat}Lu-DOTA-DGlu-Ala-Tyr-Gly-Trp-Met-Asp ↓ Phe-NH_2
^{nat}Lu-DOTA-PP-F11	None	^{nat}Lu-DOTA-$(DGlu)_6$-Ala-Tyr-Gly-Trp-Met-Asp-Phe-NH_2
	Neprilysin-1	^{nat}Lu-DOTA-$(DGlu)_6$-Ala-Tyr-Gly-Trp-Met-Asp ↓ Phe-NH_2
	Cathepsin-L	^{nat}Lu-DOTA-$(DGlu)_6$-Ala-Tyr-Gly-Trp-Met ↓ Asp-Phe-NH_2
^{nat}Lu-DOTA-PP-F11N	None	^{nat}Lu-DOTA-$(DGlu)_6$-Ala-Tyr-Gly-Trp-Nle-Asp-Phe-NH_2
	Cathepsin-L	^{nat}Lu-DOTA-$(DGlu)_6$-Ala-Tyr-Gly-Trp-Nle ↓ Asp-Phe-NH_2

↓ = cleavage site identified by liquid chromatography/mass spectrometry.

TABLE 2
B_{max} and K_d Estimated by Saturation Binding Experiments on Intact Cells

Parameter	$^{177/nat}$Lu-DOTA-MG11	$^{177/nat}$Lu-DOTA-PP-F11	$^{177/nat}$Lu-DOTA-PP-F11N
MZ-CRC-1*			
B_{max} (nM)	0.83 ± 0.05	1.21 ± 0.10	0.94 ± 0.08
K_d (nM)	34.2 ± 4.6	33.6 ± 7.0	31.2 ± 6.9
A431-CCKR2(+)†			
B_{max} (nM)	0.54 ± 0.09	0.65 ± 0.06	0.54 ± 0.10
K_d (nM)	45.6 ± 15.4	41.7 ± 9.7	50.0 ± 7.3

*n = 3 (triplicated).
†n = 2 (triplicated).
Data are mean ± SD.

Binding and Internalization Studies

Table 2 shows the maximum number of binding sites (B_{max}) and the dissociation constant (K_d) of all radiotracers in MZ-CRC-1 and A431-CCK2R(+) cells. All 3 radiotracers showed higher B_{max} and slightly better affinity in the human-derived MZ-CRC-1 cells than in the transfected ones (B_{max}, 0.8–1.2 vs. 0.54–0.65 nM, respectively; K_d, 30–35 vs. 40–50 nM, respectively). No significant differences were observed among the radiotracers within the same cell line.

^{177}Lu-DOTA-PP-F11N showed a 1.7-times-higher internalization in MZ-CRC-1 cells (32.0% ± 1.0%) than in ^{177}Lu-DOTA-MG11 cells (18.9% ± 0.1%) at 4 h (Supplemental Fig. 1). Both radiotracers were almost exclusively internalized (<2% cell surface bound), indicating agonistic properties.

Biodistribution Studies

The biodistribution results of ^{177}Lu-DOTA-PP-F11N without and with the enzyme inhibitors are in Table 3, and the corresponding results of ^{177}Lu-DOTA-MG11 and ^{177}Lu-DOTA-PP-F11 are in Supplemental Table 2. For direct comparison, the tumor, kidney, and stomach uptake of all investigated combinations are in Table 4.

^{177}Lu-DOTA-PP-F11N had the same uptake as ^{177}Lu-DOTA-PP-F11 in all tissues and in A431-CCK2R(+) tumors, whereas it was almost double in the MZ-CRC-1 tumors (20.7 ± 1.71 vs. 11.2 ± 2.94 %IA/g, P = 0.0002). Uptake in the kidneys was 5.75 ± 1.56 %IA/g, attributed to urinary excretion, followed by the CCK2R-positive stomach (2.15 ± 0.83 %IA/g). Uptake in all other tissues was low, contributing to very low background radioactivity.

Significantly higher accumulation of all 3 radiotracers was found in MZ-CRC-1 tumors than in A431-CCK2R(+) (Table 4). Uptake in MZ-CRC-1 tumors was approximately double that in ^{177}Lu-DOTA-MG11 (3.17 ± 1.47 vs. 1.45 ± 0.30 %IA/g, P = 0.0190) and ^{177}Lu-DOTA-PP-F11 (11.2 ± 2.94 vs. 6.70 ± 0.56 %IA/g, P = 0.0104) and up to 3 times higher than that in ^{177}Lu-DOTA-PP-F11N (20.7 ± 1.71 vs. 6.94 ± 0.82% IA/g, P < 0.0001). The highest uptake observed was for ^{177}Lu-DOTA-PP-F11N in MZ-CRC-1 tumors.

TABLE 3
Biodistribution Results of ^{177}Lu-DOTA-PP-F11N Without and With Phosphoramidon and Thiorphan in Nude Mice Bearing A431-CCK2R(+) and MZ-CRC-1 Xenografts

Organ	^{177}Lu-DOTA-PP-F11N	^{177}Lu-DOTA-PP-F11N + phosphoramidon	^{177}Lu-DOTA-PP-F11N + thiorphan
Blood	0.02 ± 0.00	0.01 ± 0.00	0.01 ± 0.00
Heart	0.02 ± 0.01	0.02 ± 0.01	0.02 ± 0.02
Lung	0.04 ± 0.02	0.05 ± 0.02	0.03 ± 0.02
Liver	0.12 ± 0.02	0.07 ± 0.01	0.19 ± 0.09
Pancreas	0.07 ± 0.03	0.07 ± 0.02	0.06 ± 0.03
Spleen	0.05 ± 0.03	0.02 ± 0.01	0.08 ± 0.03
Stomach	2.15 ± 0.83	2.15 ± 0.55	2.68 ± 0.80
Intestine	0.10 ± 0.08	0.09 ± 0.05	0.09 ± 0.06
Kidney	5.75 ± 1.56	5.21 ± 0.78	6.29 ± 1.51
Muscle	0.04 ± 0.03	0.03 ± 0.02	0.03 ± 0.02
Bone	0.22 ± 0.17	0.29 ± 0.14	0.45 ± 0.35
A431-CCK2R(+)	6.94 ± 0.82	8.53 ± 2.22	10.01 ± 2.78
MZ-CRC-1	20.68 ± 1.71	15.56 ± 3.80	21.82 ± 4.17

Data are mean %IA/g ± SD (n = 5–6) 4 h after injection.

TABLE 4
Tumor, Kidney, and Stomach Uptake of 3 Investigated Radiotracers Without or With Phosphoramidon or Thiorphan in Nude Mice Bearing A431-CCK2R(+) and MZ-CRC-1 Xenografts

Radiotracer	Control	+ Phosphoramidon	*P*	+ Thiorphan	*P*
^{177}Lu-DOTA-MG11					
A431-CCK2R(+)	1.45 ± 0.30	7.34 ± 1.64	<0.0001	5.38 ± 1.36	<0.0001
MZ-CRC-1	3.17 ± 1.47	17.24 ± 4.81	<0.0001	12.41 ± 4.20	0.0007
Kidneys	1.08 ± 0.15	1.36 ± 0.24	0.0056	1.33 ± 0.41	0.1465
Stomach	1.06 ± 0.23	4.04 ± 0.74	<0.0001	3.05 ± 0.83	<0.0001
^{177}Lu-DOTA-PP-F11					
A431-CCK2R(+)	6.70 ± 0.56	9.34 ± 1.11	0.0014	8.68 ± 1.18	0.0096
MZ-CRC-1	11.16 ± 2.94	19.72 ± 4.68	0.0085	8.09 ± 2.17	0.1905*
Kidneys	4.30 ± 0.56	5.50 ± 0.77	0.0008	6.56 ± 0.86	<0.0001*
Stomach	2.18 ± 0.95	1.72 ± 0.22	0.3227	2.20 ± 0.39	0.9628
^{177}Lu-DOTA-PP-F11N					
A431-CCK2R(+)	6.94 ± 0.82	8.53 ± 2.22	0.0855	10.01 ± 2.78	0.0114
MZ-CRC-1	20.68 ± 1.71	15.56 ± 3.80	0.0215	21.82 ± 4.17	0.5868
Kidneys	5.75 ± 1.56	5.21 ± 0.78	0.1346	6.29 ± 1.51	0.0002*
Stomach	2.15 ± 0.83	2.15 ± 0.55	0.9979	2.68 ± 0.80	0.1511

*Calculated using Mann–Whitney. *P* values are with reference to control group of each radiotracer.
Data are mean %IA/g ± SD (n = 5–6) 4 h after injection.

Coinjection of phosphoramidon or thiorphan with ^{177}Lu-DOTA-MG11 increased the uptake in A431-CCK2R(+) tumors by a factor of 5 and 3.7, respectively, and in MZ-CRC-1 tumors by a factor of 5.4 and 3.9, respectively (Table 4). However, stomach uptake was also increased (3.8-fold and 2.9-fold, respectively), whereas kidney uptake remained unchanged. Less profound was the effect of phosphoramidon on ^{177}Lu-DOTA-PP-F11, resulting in an increase by a factor of only 1.4 in A431-CCK2R(+) tumors and only 1.8 in MZ-CRC-1 tumors, whereas thiorphan resulted in a slight improvement (1.3-fold in A431-CCK2R(+)) or even reduction (1.4 times in MZ-CRC-1) (Table 4). Kidney and stomach uptake was not affected by the use of any of the inhibitors. In contrast to these findings, phosphoramidon did not influence uptake of ^{177}Lu-DOTA-PP-F11N in A431-CCK2R(+) tumors (6.94 ± 0.82 vs. 8.53 ± 2.22 %IA/g, $P > 0.05$), whereas it even induced a reduction in MZ-CRC-1 xenografts (20.7 ± 1.71 vs. 15.6 ± 3.80 % IA/g, $P < 0.05$). Thiorphan improved uptake in A431-CCK2R(+) (6.94 ± 0.82 vs. 10.0 ± 2.78 %IA/g, $P < 0.05$) but not in MZ-CRC-1 (20.7 ± 1.71 vs. 21.8 ± 4.17 %IA/g, $P > 0.05$). Interestingly, the protease inhibitors increased the SD for uptake of all radiotracers, compared with pure radiotracer injections.

NanoSPECT/CT Imaging and Autoradiography

NanoSPECT/CT images 4 h after injection of ^{177}Lu-DOTA-PP-F11N (Figs. 1A and 1B) and ^{177}Lu-DOTA-PP-F11N + phosphoramidon (Figs. 1C and 1D) in MZ-CRC-1 and A431-CCK2R(+) and dual xenografts showed a higher and more homogeneous uptake in MZ-CRC-1 tumors than in A431-CCK2R(+).

In line with imaging, autoradiography indicated an inhomogeneous distribution of ^{177}Lu-DOTA-PP-F11N in the A431-CCK2R(+) xenograft, linked to central necrosis and hemorrhage (Figs. 2A–2C), whereas MZ-CRC-1 tumors revealed a more uniform tumor architecture and distribution (Figs. 2A–2C).

First-in-Human Data

SPECT and SPECT/CT images revealed highly ^{177}Lu-DOTA-PP-F11N–avid recurrent disease in the left thyroid bed and in 3 lymph node metastases (Figs. 3A and 3B), indicating sufficient stability. The high stomach uptake was attributed to the high density of CCK2R located on enterochromaffin-like cells in the corpus

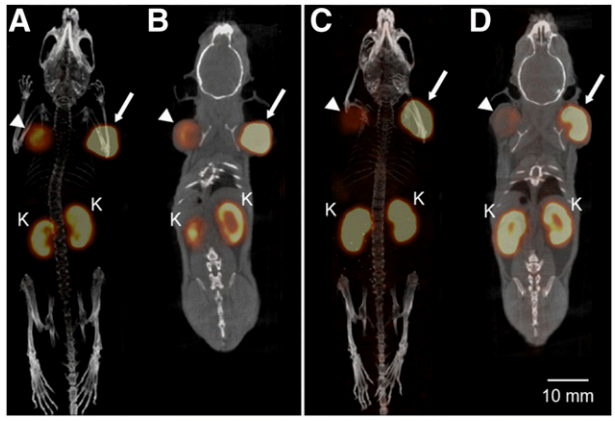

FIGURE 1. NanoSPECT/CT images of ^{177}Lu-DOTA-PP-F11N without (A and B) and with (C and D) coinjection of phosphoramidon in dual tumor model using A431-CCK2R(+) xenograft (arrowhead) on right shoulder and MZ-CRC-1 xenograft (arrow) on left shoulder. Maximum-intensity projections (A and C) reveal low uptake in A431-CCK2R(+) tumors and high uptake in MZ-CRC-1 tumors, even though SPECT/CT images (B and D) reveal that tumor size is approximately the same. Very low background and high image contrast were achieved, without significant uptake in other excreting organs, besides kidneys (K). No difference in tumor or organ uptake was noticed with and without phosphoramidon.

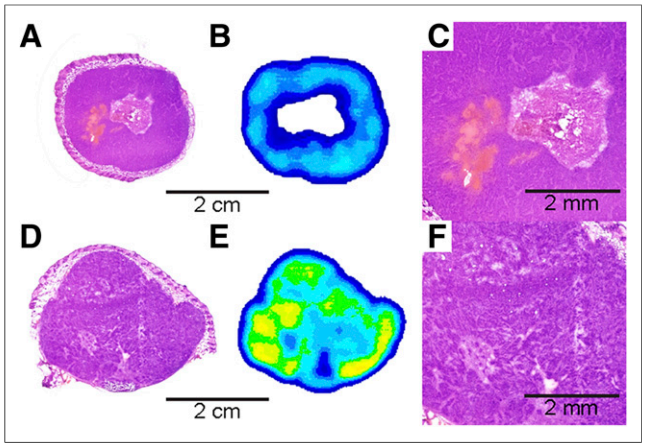

FIGURE 2. Autoradiography and hematoxylin-and-eosin histology of ^{177}Lu-DOTA-PP-F11N in A431-CCK2R(+) (A–C) and MZ-CRC-1 (D–F) tumors. Radiotracer distribution in A431-CCK2R(+) is inhomogeneous, with low uptake in tumor core (A) that is linked to necrosis and hemorrhage (B and C). Radiotracer distribution in MZ-CRC-1 is much more homogeneous (D), and no relevant areas of necrosis or hemorrhage can be detected (E and F).

mucosa of the stomach. In addition, ^{177}Lu-DOTA-PP-F11N accumulation was also seen in the colon, kidneys, and urinary bladder. The tumor localizations were confirmed by ^{18}F-DOPA PET/CT, the current gold standard for imaging of metastasized MTC.

DISCUSSION

Radiolabeled gastrin analogs can potentially provide a long-needed tool for diagnosis and therapy (theranostics) of MTC. Peptide stabilization either chemically or in situ (*12*) may deliver a higher dose to the tumor; therefore, it is essential to know which approach enhances the therapeutic effect and whether the combination has a synergistic effect. We aimed to answer this question and to optimize the therapeutic efficacy of radiolabeled gastrin analogs, focusing on ^{177}Lu-DOTA-PP-F11N.

Several extracellular proteases have been suspected to degrade gastrin and its analogs, with neprilysin being one of the main enzymes (*16–19*). We studied a panel of extracellular and intracellular endoproteases, in addition to the published proteases. We confirmed that neprilysins cleave ^{nat}Lu-DOTA-MG11 between Gly-Trp and Asp-Phe (*11*). Asp-Phe cleavage from neprilysin-1 was also found for ^{nat}Lu-DOTA-PP-F11. Interestingly, ^{nat}Lu-DOTA-PP-F11N was not cleaved, possibly because of the replacement of methionine by norleucine, making the peptide less of a substrate for the neprilysins. Despite in vitro indications that gastrin analogs with less than 2 Glu residues are angiotensin-converting enzyme–sensitive (*17*), we found no degradation with the $(\text{D}Glu)_6$ or $(\text{D}Glu)_1$ analogs by angiotensin-converting enzyme 1 or endothelin-converting enzyme 1. Our data are in line with Kaloudi et al. (*13*), indicating that angiotensin-converting enzyme is not involved in the catabolism of ^{111}In-DOTA-MG11, probably because of the conjugation of ^{nat}Lu-DOTA to D-glutamic acid. ^{nat}Lu-DOTA-MG11 was liable against the intracellular cysteine proteases cathepsin-B and -C, whereas the 2 other analogs are protected, potentially because of the negatively charged residues of the $(\text{D}Glu)_6$ extending their peptide sequence. The same is true for the liability against cathepsin-S. However, all analogs were found to be cleaved by cathepsin-L. These results might be translatable into in vivo because proteolysis may also happen intracellularly and adjacent to the tumor. Indeed, other classes of proteases are overexpressed by tumor cells; for example, matrix metalloproteases, serine and cysteine proteases, such as cathepsins, and their overexpression seem to play an important role in cancer progression by facilitating tissue invasion (*20–22*). Our results suggest that the intracellular cysteine cathepsin-C and -L might be involved in the degradation of the metallated gastrin analogs.

The MZ-CRC-1 tumors accumulated higher amounts of ^{177}Lu-DOTA-MG11, ^{177}Lu-DOTA-PP-F11, and ^{177}Lu-DOTA-PP-F11N than did the A431-CCK2R(+), as can be explained by their higher B_{max} (1.5–1.9 times). Autoradiography showed that MZ-CRC-1 tumors, besides being higher, also have homogeneous ^{177}Lu-DOTA-PP-F11N uptake, compared with A431-CCK2R(+). The differences among ^{177}Lu-DOTA-MG11, ^{177}Lu-DOTA-PP-F11, and ^{177}Lu-DOTA-PP-F11N within the same xenograft model (MZ-CRC-1 or A431-CCK2R(+)) are attributed mainly to their varying in vivo stability. This possibility is supported by their similar K_d and B_{max} for each individual cell line. However, in vitro internalization studies indicate higher internalization of ^{177}Lu-DOTA-PP-F11N in MZ-CRC-1 cells than in the reference ^{177}Lu-DOTA-MG11, a finding that may also argue for its better performance. The human-derived MTC cell line MZ-CRC-1 is used for first time in the in vivo evaluation of gastrin analogs. The findings are significant because this tumor model might be more realistic and closer to the MTC in humans.

The use of protease inhibitors has a significant impact on the in vivo stability and tumor uptake of highly unstable gastrin-based radiotracers, such as ^{177}Lu-DOTA-MG11. However, this effect cannot be documented for stabilized analogs such as ^{177}Lu-DOTA-PP-F11N. In addition, it is possible that

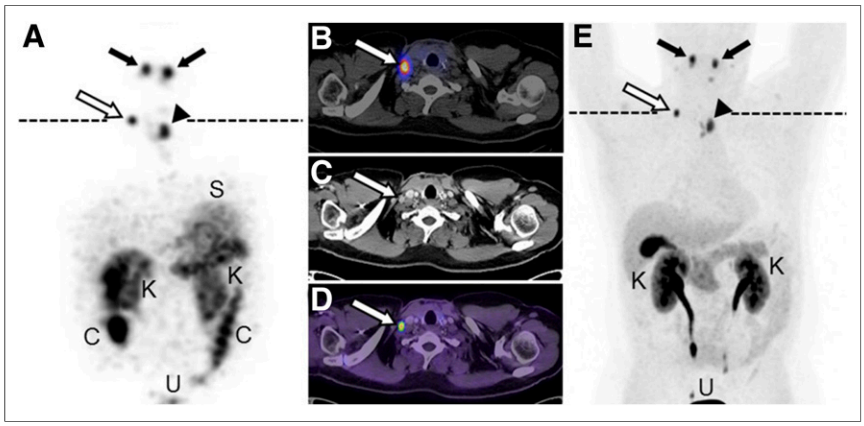

FIGURE 3. Patient with metastatic MTC, whole-body SPECT (A) and transaxial SPECT/CT (B) images 24 h after injection of 1,071 MBq of ^{177}Lu-DOTA-PP-F11N; contrast medium–enhanced transaxial CT image (C); and transaxial PET/CT (D) and whole-body PET (E) images 30 min after injection of 230 MBq of ^{18}F-DOPA. Dashed lines indicate level of transaxial slices. SPECT and SPECT/CT show highly ^{177}Lu-DOTA-PP-F11N–avid recurrent disease in left thyroid bed (arrowhead), 2 retropharyngeal lymph node metastases (black arrows) and 1 right supraclavicular lymph node metastasis with diameter of 1 cm (white arrow). This finding was confirmed by CT and ^{18}F-DOPA PET/CT. Whole-body SPECT shows additional ^{177}Lu-DOTA-PP-F11N accumulation in stomach (S), kidneys (K), colon (C), and urinary bladder (U).

phosphoramidon has an influence not only on intravascular neprilysin but also on the xenografted tumor itself. It was shown that phosphoramidon lowers tumor cell invasion and growth by altering the balance between proteolysis and protease inhibition in the processes of the extracellular matrix (*23*). Importantly, the highest tumor uptake was found for the ^{177}Lu-DOTA-PP-F11N in MZ-CRC-1 tumors, without using any inhibitor, reaching an uptake similar to the one achieved by ^{177}Lu-DOTA-MG11 + phosphoramidon and ^{177}Lu-DOTA-PP-F11 + phosphoramidon. Regarding tumor-to-kidney ratio, ^{177}Lu-DOTA-MG11 + phosphoramidon performed better (^{177}Lu-DOTA-MG11 + phosphoramidon [12.6] > ^{177}Lu-DOTA-PP-F11N = ^{177}Lu-DOTA-PP-F11+phosphoramidon [3.6], considering the MZ-CRC-1 tumor). Our new findings, including the data of the reference radiotracers ^{177}Lu-DOTA-MG11 and ^{177}Lu-DOTA-PP-F11, are in line with the literature reporting on ^{111}In-DOTA-MG11 and ^{111}In-DOTA-PP-F11N (*13,24*). In addition, they indicate that the radiometal is not influencing the in vivo uptake of radiolabeled gastrin analogs, as seen with other radiopeptides.

The results of this study were encouraging regarding the clinical translation of this radiotracer, as its potential might be higher than expected. A phase 0 clinical study (LUMED) currently ongoing in our hospital is investigating the ability of ^{177}Lu-DOTA-PP-F11N to visualize MTC metastases in a small cohort of MTC patients. We found high ^{177}Lu-DOTA-PP-F11N accumulation in the tumors, kidneys, and stomach. The high gastric uptake might spotlight this organ as a potential dose-limiting factor besides the kidneys. Taking this into consideration, the superiority of the combination ^{177}Lu-DOTA-MG11 + phosphoramidon based on tumor-to-kidney ratio is compensated by the superiority of ^{177}Lu-DOTA-PP-F11N in terms of tumor-to-stomach ratio (4.3 vs. 9.6, respectively, in xenografts). Importantly, potential side effects (especially long-term) of protease inhibitors, and especially of neprilysin inhibitors, are not well understood and, for example, could potentially interact with the development of Alzheimer disease and cancer (*25*).

CONCLUSION

^{177}Lu-DOTA-PP-F11N reaches a tumor uptake that ^{177}Lu-DOTA-MG11 can achieve only in combination with inhibitors. The application of single radiotracers in humans without additives is less demanding and facilitates clinical translation, licensing, and clinical acceptance. Moreover, the use of enzyme inhibitors considerably increases the stomach uptake, which might be relevant as indicated by first clinical results. Therefore, chemical stabilization is preferable over in situ stabilization, whereas a synergistic effect, if any, when combining both approaches is limited for highly stabilized analogs. The potential side effects of inhibitors and their unknown effects on the tumor microenvironment further support the use of stabilized radiotracers as first choice. The outcome of this study is relevant for different peptide families and their clinical translation.

DISCLOSURE

The study was financially supported by the University of Basel (Nachwuchsförderung Klinische Forschung), Swiss cancer research (KFS-3170-02-2013), and the Nora van Meeuwen-Haefliger Stiftung, Basel. No other potential conflict of interest relevant to this article was reported.

ACKNOWLEDGMENTS

We thank Dr. Luigi Aloj (Istituto Nazionale Tumori "Fondazione G. Pascale"–IRCCS, Napoli, Italy) and Prof. K.R. Alexander Knuth (National Center for Cancer Care and Research NCCCR, Hamad Medical Corporation, Doha, Qatar; formerly Internal Medicine/Oncology, University of Zurich, Switzerland) for kindly providing us with the A431-CCKR(−/+) and MZ-CRC-1 cell lines, respectively. We thank Luigi Del Pozzo and Dr. Ibai Valverde for their support and ITM (Munich, Germany) for kindly providing $^{177}LuCl_3$.

REFERENCES

1. Moley JF, Fialkowski EA. Evidence-based approach to the management of sporadic medullary thyroid carcinoma. *World J Surg.* 2007;31:946–956.
2. Hadoux J, Pacini F, Tuttle RM, Schlumberger M. Management of advanced medullary thyroid cancer. *Lancet Diabetes Endocrinol.* 2016;4:64–71.
3. Ernani V, Kumar M, Chen AY, Owonikoko TK. Systemic treatment and management approaches for medullary thyroid cancer. *Cancer Treat Rev.* 2016;50:89–98.
4. Wells SA, Asa SL, Dralle H, et al. Revised American Thyroid Association guidelines for the management of medullary thyroid carcinoma. *Thyroid.* 2015;25:567–610.
5. Reubi JC, Schaer JC, Waser B. Cholecystokinin(CCK)-A and CCK-B/gastrin receptors in human tumors. *Cancer Res.* 1997;57:1377–1386.
6. Behr TM, Behe MP. Cholecystokinin-B/gastrin receptor-targeting peptides for staging and therapy of medullary thyroid cancer and other cholecystokinin-B receptor-expressing malignancies. *Semin Nucl Med.* 2002;32:97–109.
7. Good S, Walter MA, Waser B, et al. Macrocyclic chelator-coupled gastrin-based radiopharmaceuticals for targeting of gastrin receptor-expressing tumours. *Eur J Nucl Med Mol Imaging.* 2008;35:1868–1877.
8. Roosenburg S, Laverman P, van Delft FL, Boerman OC. Radiolabeled CCK/gastrin peptides for imaging and therapy of CCK2 receptor-expressing tumors. *Amino Acids.* 2011;41:1049–1058.
9. Kolenc-Peitl P, Mansi R, Tamma M, et al. Highly improved metabolic stability and pharmacokinetics of indium-111-DOTA-gastrin conjugates for targeting of the gastrin receptor. *J Med Chem.* 2011;54:2602–2609.
10. Laverman P, Joosten L, Eek A, et al. Comparative biodistribution of 12 ^{111}In-labelled gastrin/CCK2 receptor-targeting peptides. *Eur J Nucl Med Mol Imaging.* 2011;38:1410–1416.
11. Ocak M, Helbok A, Rangger C, et al. Comparison of biological stability and metabolism of CCK2 receptor targeting peptides, a collaborative project under COST BM0607. *Eur J Nucl Med Mol Imaging.* 2011;38:1426–1435.
12. Nock BA, Maina T, Krenning EP, de Jong M. "To serve and protect": enzyme inhibitors as radiopeptide escorts promote tumor targeting. *J Nucl Med.* 2014;55:121–127.
13. Kaloudi A, Nock BA, Lymperis E, et al. Impact of clinically tested NEP/ACE inhibitors on tumor uptake of [^{111}In-DOTA]MG11: first estimates for clinical translation. *EJNMMI Res.* 2016;6:15.
14. Aloj L, Aurilio M, Rinaldi V, et al. Comparison of the binding and internalization properties of 12 DOTA-coupled and ^{111}In-labelled CCK2/gastrin receptor binding peptides: a collaborative project under COST action BM0607. *Eur J Nucl Med Mol Imaging.* 2011;38:1417–1425.
15. Bozkurt MF, Virgolini I, Balogova S, et al. Guideline for PET/CT imaging of neuroendocrine neoplasms with ^{68}Ga-DOTA-conjugated somatostatin receptor targeting peptides and ^{18}F-DOPA. *Eur J Nucl Med Mol Imaging.* 2017;44:1588–1601.
16. Noble F, Wank SA, Crawley JN, et al. International union of pharmacology. XXI. Structure, distribution, and functions of cholecystokinin receptors. *Pharmacol Rev.* 1999;51:745–781.
17. Dubreuil P, Fulcrand P, Rodriguez M, Fulcrand H, Laur J, Martinez J. Novel activity of angiotensin-converting enzyme: hydrolysis of cholecystokinin and gastrin analogues with release of the amidated C-terminal dipeptide. *Biochem J.* 1989;262:125–130.
18. Pauwels S, Najdovski T, Dimaline R, Lee CM, Deschodt-Lanckman M. Degradation of human gastrin and CCK by endopeptidase 24.11: differential behaviour of the sulphated and unsulphated peptides. *Biochim Biophys Acta.* 1989;996:82–88.
19. Deschodt-Lanckman M, Pauwels S, Najdovski T, Dimaline R, Dockray GJ. In vitro and in vivo degradation of human gastrin by endopeptidase 24.11. *Gastroenterology.* 1988;94:712–721.
20. Egeblad M, Werb Z. New functions for the matrix metalloproteinases in cancer progression. *Nat Rev Cancer.* 2002;2:161–174.
21. Joyce JA, Hanahan D. Multiple roles for cysteine cathepsins in cancer. *Cell Cycle.* 2004;3:1516–1619.
22. Mohamed MM, Sloane BF. Cysteine cathepsins: multifunctional enzymes in cancer. *Nat Rev Cancer.* 2006;6:764–775.
23. Pross M, Lippert H, Mantke R, et al. A proteinase inhibitor decreases tumor growth in a laparoscopic rat model. *Surg Endosc.* 2001;15:882–885.
24. Kaloudi A, Nock BA, Lymperis E, Krenning EP, de Jong M, Maina T. Improving the in vivo profile of minigastrin radiotracers: a comparative study involving the neutral endopeptidase inhibitor phosphoramidon. *Cancer Biother Radiopharm.* 2016;31:20–28.
25. Galli A, Lombardi F. Neprilysin inhibition for heart failure. *N Engl J Med.* 2014;371:2335.